actuators

MDPI

Article

Model Predictive Position Control of Tubular Permanent Magnet Linear Synchronous Motor for Precision Positioning Based on Neural Network Model Reference Adaptive Disturbance Observer

Yuzhe Zhao, Zhitai Liu * and Rengui Qiu

Research Institute of Intelligent Control and Systems, Harbin Institute of Technology, Harbin 150001, China; yuzhezhao@stu.hit.edu.cn (Y.Z.); 23b904002@stu.hit.edu.cn(R.Q.)
* Correspondence: ztliu@hit.edu.cn

Abstract

To improve the dynamic performance of position tracking in permanent magnet synchronous linear motors, a model predictive position control method based on disturbance observer is proposed. Firstly, a novel neural network enhanced model reference adaptive observer is designed to estimate the lumped disturbance of the system. Taking the estimated disturbance as a new state variable, it is explicitly embedded in the framework of model prediction, which realizes the online estimation and compensation of disturbance, and effectively solves the deterioration of control performance caused by inaccurate system parameters and unknown disturbance in model prediction method. The increment of the control input is used as the input of the prediction equation, which makes the control input smoother and avoids drastic changes. The adaptive gain of the observer is designed by Lyapunov theory and the stability of the system is analyzed. A large number of experiments and analysis are carried out on the tubular permanent magnet linear synchronous motor platform, which proves the effectiveness of the proposed method.

Keywords: permanent magnet linear synchronous motor; trajectory tracking; neural networks; adaptive disturbance observer; model predictive position control

1. Introduction

Permanent magnet linear synchronous motor has been widely used in machine tools, semiconductor manufacturing equipment and other occasions requiring high-precision trajectory tracking because of its high efficiency, high power density and fast dynamic response [1–5]. The operation environment of industrial equipment is complex, and disturbance and uncertainty are inevitable [6–11]. How to realize robust precise position tracking is still the focus of current research.

The three closed-loop cascade structure combined with PID controller is the most commonly used position control method with low model dependence, limited calculation and easy engineering implementation [12]. However, when parameters change drastically or external disturbances are severe, there will be obvious problems with insufficient robustness and response lag. To address the aforementioned issues and improve the position tracking accuracy and parameter robustness of linear motor systems, some advanced control methods have been employed for motor position control [13–22]. In [13], a new composite position control strategy is proposed. The position controller is designed using

Check for updates

Academic Editors: Giorgio Olmi, Dario Croccolo and Mattia Mele

Received: 31 March 2026
Revised: 27 April 2026
Accepted: 30 April 2026
Published: 3 May 2026

Copyright: © 2026 by the authors. Licensee MDPI, Basel, Switzerland. This article is an open access article distributed under the terms and conditions of the Creative Commons Attribution (CC BY) license.

the continuous torsion algorithm (CTA) and the disturbance observer is constructed using the improved super torsion algorithm (STA) to compensate for the total disturbance, which effectively improves the dynamic performance of the system. In [17], a control method based on integral sliding mode observer (ISMO) was proposed, which effectively improved the anti-disturbance capability and tracking performance of the linear motor (LM) system. In order to improve the transient performance of the system, ref. [19] combined the traditional robust control and PID control methods and designed a new model-based robust control scheme. Reference [22] proposed a segmented iterative learning control algorithm that includes an initial error correction function, which can effectively suppress periodic interference and achieve high-precision trajectory tracking. In addition, with the continuous improvement of digital processor performance, model predictive control (MPC) has been widely used in the field of motor control [23–26]. Based on the system model to predict future dynamics, the current optimal control output can be solved by online rolling optimization, which can achieve higher dynamic response and position tracking accuracy.

Although MPC has obvious advantages in tracking accuracy, dynamic response and constraint processing, the final control performance is strongly dependent on the accuracy of the model. In practical applications, system parameter variations and external disturbances are inevitable, necessitating compensation for these unknown factors to prevent degraded control performance or even system instability. At present, the parameter robustness of MPC is mainly improved by online identification of model parameters and updating the prediction matrix [27,28], or by treating all uncertainties as centralized disturbances and compensating the disturbance values through observer estimation [29,30]. In [31], a long-term memory recursive least squares (LTM-RLS) current estimator for finite set model predictive control (FCS-MPC) was proposed, effectively improving the transient and steady-state control performance of FCS-MPC. The data-driven RLS online model identification method introduced in [32] achieves better control performance for FCS-MPC compared to offline lookup table (LUT) approaches. A robust continuous-time model predictive control (CTMPC) was proposed in [29], where an enhanced internal model disturbance observer estimates and compensates for centralized disturbances, enhancing system dynamic response and parameter robustness. Ref. [33] introduced a composite MPC method incorporating friction and disturbance information, fitting an approximate friction model and designing an extended state observer (ESO) to estimate centralized disturbances, enabling high-precision speed tracking control. However, online parameter identification requires a lot of computation, and disturbance extended MPC is more suitable for embedded systems with limited computing resources.

Therefore, this article proposes a disturbance extended model predictive position control method, which regards the disturbance as an extended state and introduces a disturbance observer to improve the dynamic tracking performance and disturbance rejection ability of the system. The input increment MPC (Δu-MPC) is used to suppress the drastic change of control input. A novel neural network enhanced model reference adaptive observer (NNMRAO) is designed to realize the online estimation of high-frequency and nonlinear disturbances. The parameter robustness of the system is significantly improved by substituting the estimated unknown disturbance into the disturbance extended MPC. The proposed method is tested on the tubular permanent magnet linear synchronous motor (TPMLSM) experimental platform, and the effectiveness of the proposed method is verified by comparative experiments.

The remaining chapters of this article are arranged as follows. Section 2 presents the dynamic equation of TPMLSM. Section 3 presents the mathematical derivation of the input incremental disturbance extended model prediction. Section 4 designs a neural network-enhanced model reference adaptive observer, derives the adaptive law using Lyapunov

theory, and analyzes the stability of the system. Section 5 presents the experimental verification process.

2. Dynamic Modeling of Tubular Permanent Magnet Synchronous Linear Motors

The mover of permanent magnet linear synchronous motor moves in a straight line along the guide rail. The motion equation is as follows

$$\begin{aligned} \frac{dx}{dt} &= v, \\ \frac{dv}{dt} &= -\frac{B}{M}v - \frac{F_c}{M}\mathrm{sgn}(v) + \frac{u}{M} - \frac{F_l}{M} - \frac{d}{M} \end{aligned} \tag{1}$$

where v and x are velocity and displacement, respectively. M is the total mass of the mover and load, B is the viscous friction coefficient, and F_c is the Coulomb friction amplitude. u denotes the control input, defined as $u = K_f * i_q$, in which K_f represents the thrust coefficient and i_q denotes the *q-axis* current. F_l refers to load thrust fluctuation, and d refers to unmodeled dynamics such as end effect. Select the state variable $X = [x, v]^T$, and the system state equation is as follows:

$$\begin{aligned} \dot{X} &= AX + Bu + B_c\mathrm{sgn}(C_vX) + B_d(F_l + d) \\ Y &= CX, \end{aligned} \tag{2}$$

where the system matrix A, control input matrix B, nonlinear friction matrix B_c, disturbance input matrix B_d, speed extraction matrix C_v and output rectangle C are as follows:

$$A = \begin{bmatrix} 0 & 1 \\ 0 & -\frac{B}{M} \end{bmatrix}, B = \begin{bmatrix} 0 \\ \frac{1}{M} \end{bmatrix}, B_c = \begin{bmatrix} 0 \\ -\frac{F_c}{M} \end{bmatrix}, B_d = \begin{bmatrix} 0 \\ -\frac{1}{M} \end{bmatrix}, C_v = \begin{bmatrix} 0 & 1 \end{bmatrix}, C = \begin{bmatrix} 1 & 0 \\ 0 & 1 \end{bmatrix}. \tag{3}$$

If Equation (2) is directly taken as the predictive model of model predictive control (MPC), due to the nonlinear term $\mathrm{sgn}(v)$, the optimization problem is a non convex nonlinear programming (NLP) problem, and the real-time calculation cost is high, which is not suitable for the implementation of embedded real-time controller. Therefore, this paper separates the Coulomb friction term from the prediction model through a feedforward compensation strategy, so that the internal optimization problem of MPC degenerates into a standard convex quadratic programming (QP) [34], thereby achieving efficient real-time solution while ensuring control accuracy.

3. Controller Design

To improve the position tracking accuracy of PMLSM under unknown disturbances and model parameter mismatches, a NNMRAO was designed to observe unknown disturbances, and the disturbance is explicitly embedded into the MPC controller to enhance the parameter robustness of the system. Figure 1 illustrates the position control architecture of the proposed method, in which a Model Predictive Controller (MPC) is employed to replace both the position loop and the velocity loop of the conventional cascade control structure.

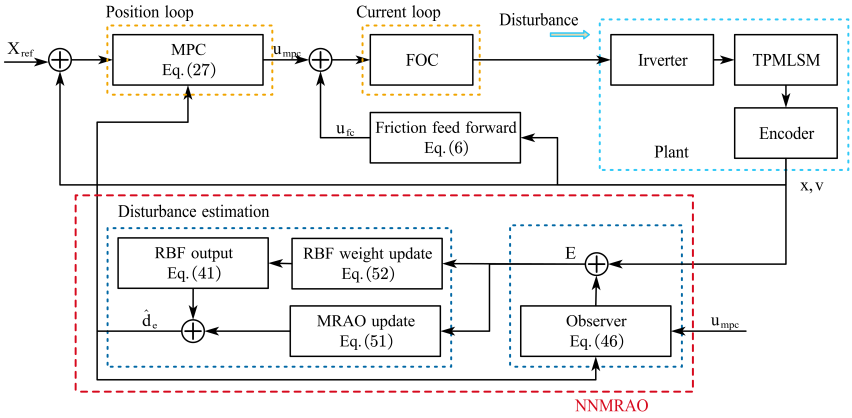


Figure 1. TPMLSM position control structure based on the proposed method.

3.1. Friction Feedforward Compensation

The total control input u is decomposed into the sum of MPC output component u_{mpc} and feedforward component u_{fc}:

$$u = u_{mpc} + u_{fc} \tag{4}$$

Substituting the above equation into Equation (1) yields:

$$\frac{dv}{dt} = -\frac{B}{M}v - \frac{F_c}{M}\mathrm{sgn}(v) + \frac{u_{mpc} + u_{fc}}{M} - \frac{F_l}{M} - \frac{d}{M} \tag{5}$$

Letting the feedforward component in the above equation cancel out the Coulomb force, we can obtain the feedforward compensation law as follows:

$$u_{fc} = F_c\mathrm{sgn}(v) \tag{6}$$

In practical systems, the value of F_c changes due to system identification errors and changes in the operating environment, making it impossible to completely and accurately offset Coulomb friction through feedforward. When the actual Coulomb friction coefficient is F_{ct}, while the nominal value used for feedforward compensation is F_c, a residual error $\Delta F_c = F_{ct} - F_c$ will exist. Substituting Equation (6) into Equation (5), the equivalent motion equation is obtained as follows:

$$\begin{aligned} \frac{dx}{dt} &= v, \\ \frac{dv}{dt} &= -\frac{B}{M}v + \frac{1}{M}u - \frac{1}{M}d_e \end{aligned} \tag{7}$$

where d_e is the equivalent lumped disturbance, $d_e = F_l + d + \Delta F_c\mathrm{sgn}(v)$.

The above equation can be rewritten in the following state-space form:

$$\begin{aligned} \dot{X} &= AX + Bu + B_d d_e \\ Y &= CX, \end{aligned} \tag{8}$$

Applying the forward Euler method [35] to discretize the above equation with sampling period T_s, the discrete-time state-space equation of the system is obtained as follows:

$$\begin{aligned} X^{k+1} &= \bar{A}X^k + \bar{B}u^k + \bar{B}_d d_e^k, \\ Y^k &= \bar{C}X^k. \end{aligned} \tag{9}$$

where $\bar{A}$, $\bar{B}$, $\bar{B}_d$ and $\bar{C}$ represent the discretized system matrices:

$$\bar{A} = \begin{bmatrix} 1 & T_s \\ 0 & 1 - \frac{T_s B}{M} \end{bmatrix}, \bar{B} = \begin{bmatrix} 0 \\ \frac{T_s}{M} \end{bmatrix}, \bar{B}_d = \begin{bmatrix} 0 \\ -\frac{T_s}{M} \end{bmatrix}, \bar{C} = \begin{bmatrix} 1 & 0 \\ 0 & 1 \end{bmatrix}. \tag{10}$$

3.2. Disturbance Extended MPC

In order to compensate for the unknown disturbance d_e, the lumped disturbance term is modeled as a slowly varying signal and extended to the system state variable. Then, the disturbance is estimated by the disturbance observer and incorporated into the MPC predictive model to improve the tracking accuracy and eliminate the steady-state bias [36]. Following the standard disturbance modeling method in MPC, assuming that the disturbance remains unchanged within the prediction range, there are:

$$d_e^{k+1} = d_e^k. \tag{11}$$

Construct an extended state containing the disturbance:

$$X_e^k = \begin{bmatrix} X^k \\ d_e^k \end{bmatrix} = \begin{bmatrix} x^k \\ v^k \\ d_e^k \end{bmatrix} \tag{12}$$

where d_e^k is estimated by the observer, the system disturbance extended state equation is as follows:

$$\begin{aligned} X_e^{k+1} &= A_e X_e^k + B_e u^k, \\ Y_e^k &= C_e X_e^k. \end{aligned} \tag{13}$$

where

$$A_e = \begin{bmatrix} \bar{A} & \bar{B}_d \\ 0 & 1 \end{bmatrix}, B_e = \begin{bmatrix} \bar{B} \\ 0 \end{bmatrix}, C_e = \begin{bmatrix} \bar{C} & 0 \end{bmatrix}. \tag{14}$$

3.3. Input Incremental MPC

In the high-precision position servo system such as tubular permanent magnet synchronous linear motor, the traditional MPC can easily cause serious current harmonics and violent thrust pulsation, and even cause structural resonance of the system due to the direct optimization of the absolute control quantity and the control of high-frequency jump of the input. In order to fundamentally suppress the above problems, the input incremental model predictive control (IMPC) architecture is introduced, and the control increment Δu^k is used as the input of the predictive model and the penalty term of the objective function. It can effectively smooth the control signal and realize the flexible operation of the system.

Define the input increment Δu^k as:

$$\Delta u^k \triangleq u^k - u^{k-1}. \tag{15}$$

The input at time k can then be expressed as:

$$u^k = u^{k-1} + \Delta u^k. \tag{16}$$

Substituting the above equation into Equation (13) yields:

$$\begin{aligned} X_e^{k+1} &= A_e X^k + B_e u^{k-1} + B_e \Delta u^k, \\ Y_e^k &= C_e X_e^k. \end{aligned} \tag{17}$$

Taking u^{k-1} as a new state variable, the augmented state vector can be obtained:

$$z^k \triangleq \begin{bmatrix} x^k \\ v^k \\ d^k \\ u^{k-1} \end{bmatrix} \tag{18}$$

The augmented state equation can be obtained as follows:

$$\begin{aligned} z^{k+1} &= \mathcal{A}z^k + \mathcal{B}\Delta u^k, \\ y^k &= \mathcal{C}z^k. \end{aligned} \tag{19}$$

The matrix coefficients are:

$$\mathcal{A} = \begin{bmatrix} \bar{A} & \bar{B}_d & \bar{B} \\ 0 & 1 & 0 \\ 0 & 0 & 1 \end{bmatrix}, \mathcal{B} = \begin{bmatrix} \bar{B} \\ 0 \\ 1 \end{bmatrix}, \mathcal{C} = \begin{bmatrix} \bar{C} & 0 & 0 \end{bmatrix} \tag{20}$$

3.4. MPC Solution

Define the prediction horizon as N_p and the control horizon as N_c. Through iterative computation, the prediction equation of the IMPC can be derived as follows:

$$\boldsymbol{Y} = \mathcal{F}z^k + \Phi\Delta\boldsymbol{U} \tag{21}$$

where $\boldsymbol{Y}$ and $\Delta\boldsymbol{U}$ represent the matrix form of output vector and control input, respectively:

$$\boldsymbol{Y} = \begin{bmatrix} y^{k+1} \\ y^{k+2} \\ y^{k+3} \\ \vdots \\ y^{k+N_p} \end{bmatrix} \tag{22}$$

$$\Delta\boldsymbol{U} = \begin{bmatrix} \Delta u^k \\ \Delta u^{k+1} \\ \Delta u^{k+2} \\ \vdots \\ \Delta u^{k+N_c-1} \end{bmatrix} \tag{23}$$

The coefficient matrix in the prediction Equation (21) is as follows:

$$\mathcal{F} = \begin{bmatrix} \mathcal{C}\mathcal{A} \\ \mathcal{C}\mathcal{A}^2 \\ \mathcal{C}\mathcal{A}^3 \\ \vdots \\ \mathcal{C}\mathcal{A}^{N_p} \end{bmatrix}, \tag{24}$$

$$\Phi = \begin{bmatrix} \mathcal{C}\mathcal{B} & 0 & \cdots & 0 \\ \mathcal{C}\mathcal{A}\mathcal{B} & \mathcal{C}\mathcal{B} & \cdots & 0 \\ \mathcal{C}\mathcal{A}^2\mathcal{B} & CAB & \cdots & 0 \\ \vdots & \vdots & \ddots & \vdots \\ \mathcal{C}\mathcal{A}^{N_p-1}\mathcal{B} & \mathcal{C}\mathcal{A}^{N_p-2}\mathcal{B} & \cdots & \mathcal{C}\mathcal{A}^{N_p-N_c}\mathcal{B} \end{bmatrix}. \tag{25}$$

The desired effect is that the system output closely tracks the reference trajectory while keeping the control increments as small as possible. By incorporating the tracking error and the control input increment as penalty terms, the following cost function is defined:

$$J = (\boldsymbol{Y} - \boldsymbol{Y}_{ref})^T \bar{Q} (\boldsymbol{Y} - \boldsymbol{Y}_{ref}) + \Delta \boldsymbol{U}^T \bar{R} \Delta \boldsymbol{U} \tag{26}$$

where $\bar{Q}$ is the output error weight matrix, $\bar{R}$ is the control increment weight matrix, and both $\bar{Q}$ and $\bar{R}$ are block diagonal matrices. $\boldsymbol{Y}_{ref}$ is the reference trajectory vector.

We need to find a $\Delta \boldsymbol{U}$ that minimizes J while satisfying the system constraints. This is a typical quadratic programming problem:

$$\begin{aligned} \min_{\Delta U} \quad & \frac{1}{2} \Delta \boldsymbol{U}^T \mathcal{H} \Delta \boldsymbol{U} + f^T \Delta \boldsymbol{U} \\ \text{s.t.} \quad & \boldsymbol{A}_{cons} \Delta \boldsymbol{U} \leq \boldsymbol{b}_{cons} \end{aligned} \tag{27}$$

Substituting the prediction Equation (21) into Equation (26) yields:

$$J = (\mathcal{F} z^k + \Phi \Delta U - \boldsymbol{Y}_{ref})^T \bar{Q} (\mathcal{F} z^k + \Phi \Delta \boldsymbol{U} - \boldsymbol{Y}_{ref}) + \Delta \boldsymbol{U}^T \bar{R} \Delta \boldsymbol{U}. \tag{28}$$

Further simplification and merging of the parts containing $\Delta \boldsymbol{U}$ yields:

$$J = \Delta \mathbf{U}^T (\Phi^T \bar{Q} \Phi + \bar{R}) \Delta \mathbf{U} + 2 \Delta \mathbf{U}^T \Phi^T \bar{Q} (\mathcal{F} z^k - \mathbf{Y}_{ref}) + \left(\mathcal{F} z^k - \mathbf{Y}_{ref} \right)^T \bar{Q} \left(\mathcal{F} z^k - \mathbf{Y}_{ref} \right) \tag{29}$$

where $(\mathcal{F} z^k - \mathbf{Y}_{ref})^T \bar{Q} \left(\mathcal{F} z^k - \mathbf{Y}_{ref} \right)$ depends only on the current state and has no effect on the solution of $\Delta \boldsymbol{U}$, it can be regarded as a constant term. Comparing with the standard quadratic programming problem Equation (26), we can obtain the coefficients:

$$\mathcal{H} = 2(\Phi^T \bar{Q} \Phi + \bar{R}) \tag{30}$$

$$f = 2 \Phi^T \bar{Q} (\mathcal{F} z^k - \mathbf{Y}_{ref}) \tag{31}$$

Apply the following constraints to the incremental control:

$$\Delta u_{min} \leq \Delta u^{k+i} \leq \Delta u_{max} \tag{32}$$

where Δu_{min} and Δu_{max} represent the upper and lower bounds of the control increment, which impose constraints on the entire control sequence and are written in matrix form:

$$\begin{bmatrix} I \\ -I \end{bmatrix} \Delta U \leq \begin{bmatrix} \Delta U_{max} \\ -\Delta U_{min} \end{bmatrix} \tag{33}$$

where ΔU_{min} and ΔU_{max} are vectors composed of Δu_{min} and Δu_{max}.

Apply constraints to the final control input:

$$u_{min} \leq u^{k+i} \leq u_{max} \tag{34}$$

where u_{min} and u_{max} are the upper and lower bounds of the control input amplitude, $u^{k+i} = u^{k-1} + \sum_{i=0}^{N_c - 1} \Delta u^i$, Write in matrix form:

$$\begin{bmatrix} L_N \\ -L_N \end{bmatrix} \Delta U \leq \begin{bmatrix} U_{max} - U_{pre} \\ -U_{min} + U_{pre} \end{bmatrix} \tag{35}$$

where U_{min}, U_{max} and U_{prev} are vectors composed of u_{min}, u_{max} and u^{k-1}, respectively, and L_N is a lower triangular matrix with all elements being 1.

Apply constraints to the system output:

$$y_{min} \leq y^{k+i} \leq y_{max} \tag{36}$$

where y_{min} and y_{max} represent the upper and lower bounds of the system output, and $\boldsymbol{Y}$ can be represented by $\Delta \boldsymbol{U}$ according to the prediction Equation (21), written in matrix form:

$$\begin{bmatrix} \Phi \\ -\Phi \end{bmatrix} \Delta U \leq \begin{bmatrix} Y_{max} - \mathcal{F} z^k \\ -Y_{min} + \mathcal{F} z^k \end{bmatrix} \tag{37}$$

where Y_{min} and Y_{max} are vectors composed of y_{min} and y_{max}.

Combining Equation (33), Equation (35), and Equation (37), the constraint matrix in Equation (26) is obtained as follows:

$$\boldsymbol{A}_{cons} = \begin{bmatrix} I \\ -I \\ L_N \\ -L_N \\ \Phi \\ -\Phi \end{bmatrix} \tag{38}$$

$$\boldsymbol{b}_{cons} = \begin{bmatrix} \Delta U_{max} \\ -\Delta U_{min} \\ U_{max} - U_{pre} \\ -U_{min} + U_{pre} \\ Y_{max} - \mathcal{F} z^k \\ -Y_{min} + \mathcal{F} z^k \end{bmatrix} \tag{39}$$

The optimal control sequence $\Delta \boldsymbol{U}$ can be obtained by solving the standard quadratic form Equation (27). The first element Δu^k is selected as the current control increment, and the current control input u_k can be obtained according to Equation (16).

4. Neural Network Model Reference Adaptive Observer

4.1. NNMRAO Structure

In order to estimate the above unknown lumped disturbance, this paper decomposes the lumped disturbance according to the following strategy:

$$d_e = d_0 + d_n, \tag{40}$$

where d_0 represents the DC or slowly varying component of the disturbance, including load bias and steady-state modeling error. d_n represents the state-dependent and time-varying nonlinear component of the disturbance, including thrust fluctuation, end effect, nonlinear friction.

In this paper, the radial basis function (RBF) neural network is used to approach d_n online. RBF is a three-layer feedforward neural network with simple structure, strong approximation ability and fast convergence speed [37,38]. The structure is shown in Figure 2.

Assumption 1. *The nonlinear disturbance d_n can be approximated online by a RBF neural network. That is, there exist an ideal weight matrix $W^* \in \mathbb{R}^N$, where N denotes the number of network nodes, and a basis function vector $\Phi(X)=[\phi_1(X),\ldots,\phi_N(X)]^T$, such that:*

$$d_n = W^{*T}\Phi(X) + \varepsilon(X) \tag{41}$$

where $\varepsilon(X)$ denotes the bounded approximation error satisfying:

$$\|\varepsilon(x)\| \le \bar{\varepsilon}. \tag{42}$$

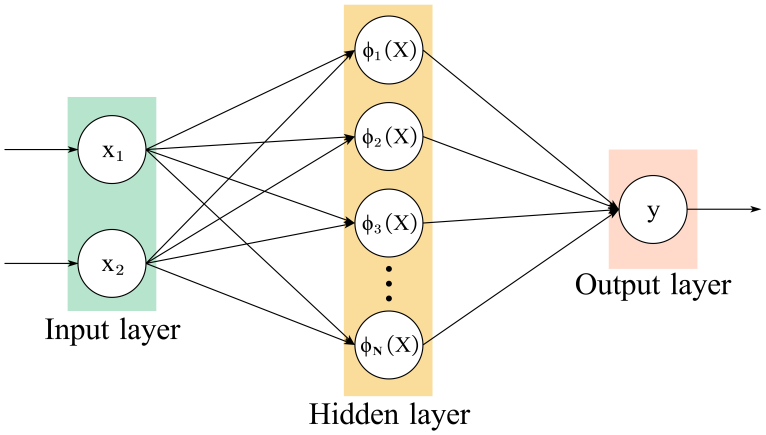


Figure 2. RBF neural network architecture.

Choose the Gaussian function as the basis function:

$$\phi_i(X) = \exp\left(-\frac{\|X - c_i\|^2}{\sigma_i^2}\right) \tag{43}$$

where c_j is the center vector of the *i-th* node, and $\sigma_j > 0$ is the width parameter. As analyzed above, the main nonlinear disturbance components that the neural network aims to approximate all depend on position and velocity. Therefore, the neural network input is selected as follows:

$$X = \begin{bmatrix} x \\ v \end{bmatrix}. \tag{44}$$

Substituting Equation (40) and Equation (41) into the original system Equation (8), the following reference model with disturbance can be obtained:

$$\dot{X} = AX + Bu + B_d d_0 + B_d W^{*T}\Phi(X) + B_d\varepsilon(X) \tag{45}$$

The NNMRAO structure is designed as follows:

$$\dot{\hat{X}} = A\hat{X} + Bu + B_d\hat{d}_0 + B_d\hat{W}^T\Phi(X) + L(X - \hat{X}) \tag{46}$$

where A, B and C are the system matrix, X is the system state, $\hat{X}$ is the estimated value of the system state, $\hat{d}_0$ is the low-frequency disturbance estimated by MRAO, $\hat{W}$ is the estimated value of the neural network weight matrix, and L is the observer gain.

Assumption 2. *The observer gain L is chosen such that the matrix $(A - L)$ is a Hurwitz stable matrix.*

4.2. NNMRAO Adaptive Law

Define the state estimation error E, the disturbance estimation error $\tilde{d}_0$, and the neural network weight estimation error $\tilde{W}$ as follows:

$$E = X - \hat{X}, \tag{47}$$

$$\tilde{d}_0 = d_0 - \hat{d}_0, \tag{48}$$

$$\tilde{W} = W^* - \hat{W}. \tag{49}$$

Subtracting the observed model Equation (46) from the reference model Equation (45) yields the error dynamic equation:

$$\dot{E} = (A - L)E + B_d\tilde{d}_0 + B_d\tilde{W}^T\Phi(X) + B_d\varepsilon(X) \tag{50}$$

To estimate the unknown disturbance d_0 and the neural network weight matrix W^*, the following adaptive update laws are designed:

$$\dot{\hat{d}}_0 = \Gamma_d B_d^T PE - \sigma_d\hat{d}_0 \tag{51}$$

$$\dot{\hat{W}} = \Gamma_W\Phi(X)E^T PB_d - \sigma_W\hat{W} \tag{52}$$

where $\Gamma_d = \Gamma_d^T > 0$ and $\Gamma_W = \Gamma_W^T > 0$ denote the learning rates of the model reference adaptive disturbance observer and the neural network, respectively. $\sigma > 0$ is the σ-modification coefficient introduced to prevent weight drift. $P = P^T > 0$ is a positive definite symmetric matrix.

4.3. NNMRAO Stability Analysis

The following Lyapunov function is constructed:

$$V = \frac{1}{2}E^T PE + \frac{1}{2}\tilde{d}_0^T\Gamma_d^{-1}\tilde{d}_0 + \frac{1}{2}\mathrm{tr}\left(\tilde{W}^T\Gamma_W^{-1}\tilde{W}\right) \tag{53}$$

Denote $V = V_1 + V_2 + V_3$, where $V_1 = \frac{1}{2}E^T PE$, $V_2 = \frac{1}{2}\tilde{d}_0^T\Gamma_d^{-1}\tilde{d}_0$, $V_3 = \frac{1}{2}\mathrm{tr}(\tilde{W}^T\Gamma_W^{-1}\tilde{W})$. Taking the time derivative of V_1 yields:

$$\dot{V}_1 = \frac{1}{2}\dot{E}^T PE + \frac{1}{2}E^T P\dot{E} \tag{54}$$

Substituting the error Equation (50) into the above expression and simplifying, one obtains:

$$\dot{V}_1 = \frac{1}{2}E^T\Big[(A - L)^T P + P(A - L)\Big]E + E^T PB_d\tilde{d}_0 + E^T PB_d\tilde{W}^T\Phi(X) + E^T PB_d\varepsilon(X) \tag{55}$$

Based on Assumption 2 and the Lyapunov matrix equation theory [39], for any given positive definite symmetric matrix $Q = Q^T > 0$, there exists a unique positive definite symmetric matrix $P = P^T > 0$ satisfying:

$$(A - L)^T P + P(A - L) = -Q \tag{56}$$

Substituting the above equation into Equation (55), one obtains:

$$\dot{V}_1 = -\frac{1}{2}E^T QE + E^T PB_d\tilde{d}_0 + E^T PB_d\tilde{W}^T\Phi(X) + E^T PB_d\varepsilon(X) \tag{57}$$

Since d_0 varies slowly and the control period is sufficiently small, it can be approximated that $\dot{d}_0 \approx 0$. Based on Equation (48), one obtains:

$$\dot{\tilde{d}}_0 = -\dot{\hat{d}}_0 \tag{58}$$

Based on the above equation and the adaptive law Equation (51), the time derivative of V_2 is obtained as follows:

$$\dot{V}_2 = \tilde{d}_0^T \Gamma_d^{-1}(-\Gamma_d B_d^T P E + \sigma_d \hat{d}_0) = -\tilde{d}_0^T B_d^T P E + \sigma_d \tilde{d}_0^T \Gamma_d^{-1} \hat{d}_0 \tag{59}$$

Since W^* is a constant matrix, it follows that $\dot{W}^* = 0$. Based on Equation (49), one obtains:

$$\dot{\tilde{W}} = -\dot{\hat{W}} \tag{60}$$

Based on the above equation and the adaptive law Equation (52), the time derivative of V_3 is obtained as follows:

$$\dot{V}_3 = \mathrm{tr}\left(\tilde{W}^T \Gamma_W^{-1}\left(-\Gamma_W \Phi E^T P B_d + \sigma \hat{W}\right)\right) = -\mathrm{tr}\left(\tilde{W}^T \Phi(X) E^T P B_d\right) + \sigma \mathrm{tr}\left(\tilde{W}^T \Gamma_W^{-1} \hat{W}\right) \tag{61}$$

Adding Equations (57), (59), and (61) together, we get:

$$\begin{aligned} \dot{V} = &-\frac{1}{2} E^T Q E + E^T P B_d \tilde{d}_0 + E^T P B_d \tilde{W}^T \Phi(X) + E^T P B_d \varepsilon(X) - \tilde{d}_0^T B_d^T P E + \sigma_d \tilde{d}_0^T \Gamma_d^{-1} \hat{d}_0 \\ &- \mathrm{tr}\left(\tilde{W}^T \Phi(X) E^T P B_d\right) + \sigma \mathrm{tr}\left(\tilde{W}^T \Gamma_W^{-1} \hat{W}\right) \end{aligned} \tag{62}$$

By combining and eliminating terms in the above equation , we can obtain:

$$\dot{V} = -\frac{1}{2} E^T Q E + E^T P B_d \varepsilon(X) + \sigma_d \tilde{d}_0^T \Gamma_d^{-1} \hat{d}_0 + \sigma\, \mathrm{tr}\left(\tilde{W}^T \Gamma_W^{-1} \hat{W}\right) \tag{63}$$

For the first term, according to the Rayleigh quotient principle [40], we can obtain:

$$-\frac{1}{2} E^T Q E \leq -\frac{\lambda_{\min}(Q)}{2} \|E\|^2 \tag{64}$$

For the neural network error approximation term $E^T P B_d \varepsilon(X)$, combining Assumption 1 and according to the Cauchy–Schwarz inequality [41], we can obtain:

$$\left\| E^T P B_d \varepsilon(X) \right\| \leq \left\| P B_d \right\| \cdot \left\| E \right\| \bar{\varepsilon} \tag{65}$$

Further, based on Young's inequality, for all $\eta > 0$, it yields:

$$\left\| E^T P B_d \varepsilon(X) \right\| \leq \frac{\eta}{2} \|E\|^2 + \frac{\|P B_d\|^2 \bar{\varepsilon}^2}{2\eta} \tag{66}$$

For the σ-modification term $\sigma_d \tilde{d}_0^T \Gamma_d^{-1} \hat{d}_0$ of the disturbance, since $\tilde{d}_0 = d_0 - \hat{d}_0$, it can be obtained that:

$$\sigma_d \tilde{d}_0^T \Gamma_d^{-1} \hat{d}_0 = \sigma_d \tilde{d}_0^T \Gamma_d^{-1} d_0 - \sigma_d \tilde{d}_0^T \Gamma_d^{-1} \tilde{d}_0. \tag{67}$$

According to Young's inequality, we can obtain:

$$\sigma_d \tilde{d}_0^T \Gamma_d^{-1} d_0 \leq \frac{\sigma_d}{2} \tilde{d}_0^T \Gamma_d^{-1} \tilde{d}_0 + \frac{\sigma_d}{2} d_0^T \Gamma_d^{-1} d_0. \tag{68}$$

Substituting the above equation into (67) yields:

$$\sigma_d \tilde{d}_0^T \Gamma_d^{-1} \hat{d}_0 \leq -\frac{\sigma_d}{2} \tilde{d}_0^T \Gamma_d^{-1} \tilde{d}_0 + \frac{\sigma_d}{2} d_0^T \Gamma_d^{-1} d_0. \tag{69}$$

For the σ-modification term $\sigma\,\mathrm{tr}(\tilde{W}^T\Gamma_W^{-1}\hat{W})$ of the weights, since $\tilde{W} = W^* - \hat{W}$, we can obtain:

$$\sigma\,\mathrm{tr}\left(\tilde{W}^T\Gamma_W^{-1}\hat{W}\right) = \sigma\,\mathrm{tr}\left(\tilde{W}^T\Gamma_W^{-1}W^*\right) - \sigma\,\mathrm{tr}\left(\tilde{W}^T\Gamma_W^{-1}\tilde{W}\right) \tag{70}$$

According to the matrix trace inequality, we can obtain:

$$\mathrm{tr}\left(\tilde{W}^T\Gamma_W^{-1}W^*\right) \le \frac{1}{2}\mathrm{tr}\left(\tilde{W}^T\Gamma_W^{-1}\tilde{W}\right) + \frac{1}{2}\mathrm{tr}\left(W^{*T}\Gamma_W^{-1}W^*\right) \tag{71}$$

Substituting the above equation into Equation (70) yields:

$$\sigma\,\mathrm{tr}\left(\tilde{W}^T\Gamma_W^{-1}\hat{W}\right) \le -\frac{\sigma}{2}\,\mathrm{tr}\left(\tilde{W}^T\Gamma_W^{-1}\tilde{W}\right) + \frac{\sigma}{2}\,\mathrm{tr}\left(W^{*T}\Gamma_W^{-1}W^*\right) \tag{72}$$

Substituting Equations (64), (66), and (72) into Equation (63) yields:

$$\begin{aligned}\dot{V} \le -\frac{1}{2}\lambda_{\min}(Q)\|E\|^2 + \frac{\eta}{2}\|E\|^2 - \frac{\sigma_d}{2}\tilde{d}_0^T\Gamma_d^{-1}\tilde{d}_0 - \frac{\sigma}{2}\mathrm{tr}\left(\tilde{W}^T\Gamma_W^{-1}\tilde{W}\right) + \frac{\|PB_d\|^2\bar{\varepsilon}^2}{2\eta} + \frac{\sigma_d}{2}d_0^T\Gamma_d^{-1}d_0 \\ + \frac{\sigma}{2}\mathrm{tr}\left(W^{*T}\Gamma_W^{-1}W^*\right)\end{aligned} \tag{73}$$

Further arrangement:

$$\dot{V} \le -\left(\frac{\lambda_{\min}(Q)}{2} - \frac{\eta}{2}\right)\|E\|^2 - \frac{\sigma_d}{2}\tilde{d}_0^T\Gamma_d^{-1}\tilde{d}_0 - \frac{\sigma_W}{2}\mathrm{tr}\left(\tilde{W}^T\Gamma_W^{-1}\tilde{W}\right) + C \tag{74}$$

where take $0 < \eta < \lambda_{\min}(Q)$, then we have $\alpha_1 = \frac{\lambda_{\min}(Q)-\eta}{2} > 0$, $\alpha_2 = \frac{\sigma_d}{2} > 0$, $\alpha_3 = \frac{\sigma_W}{2} > 0$, and the constant $C = \frac{\|PB_d\|^2\bar{\varepsilon}^2}{2\eta} + \frac{\sigma_d}{2}d_0^T\Gamma_d^{-1}d_0 + \frac{\sigma}{2}\mathrm{tr}\left(W^{*T}\Gamma_W^{-1}W^*\right) > 0$.

Define the comprehensive error:

$$\Omega = \|E\|^2 + \tilde{d}_0^T\Gamma_d^{-1}\tilde{d}_0 + \mathrm{tr}\left(\tilde{W}^T\Gamma_W^{-1}\tilde{W}\right) \tag{75}$$

Let $\alpha = \min(\alpha_1, \alpha_2, \alpha_3)$. Then the above equation can be simplified as:

$$\dot{V} \le -\alpha\Omega + C \tag{76}$$

There is an equivalent relationship between the Lyapunov function Equation (53) and the composite error metric Ω; that is, there is a normal number $\lambda_1, \lambda_2 > 0$ such that:

$$\lambda_1\Omega \le V \le \lambda_2\Omega \tag{77}$$

Substituting the above equation into Equation (76) yields:

$$\dot{V} \le -\frac{\alpha}{\lambda_2}V + C. \tag{78}$$

According to the comparison lemma [42], we can obtain:

$$V(t) \le e^{-\frac{\alpha}{\lambda_2}t}V(0) + \frac{\lambda_2 C}{\alpha}\left(1 - e^{-\frac{\alpha}{\lambda_2}t}\right) \tag{79}$$

Then we can obtain:

$$\limsup_{t\to\infty} V(t) \le \frac{\lambda_2 C}{\alpha} \tag{80}$$

According to Equation (76), we can further obtain:

$$\limsup_{t\to\infty} \Omega(t) \le \frac{\lambda_2}{\lambda_1}\frac{C}{\alpha} \tag{81}$$

The above results indicate that when the neural network approximation error is bounded, the adaptive law correction term exists, and the slowly varying component d_0 of the lumped disturbance satisfies $\dot{d}_0 \approx 0$, the composite error vector $(E, \tilde{d}_0, \tilde{W})$ is uniformly ultimately bounded (UUB) and eventually enters the compact set $\mathcal{D}$:

$$\mathcal{D} = \left\{ (E, \tilde{d}_0, \tilde{W}) | \Omega \leq \frac{\lambda_2}{\lambda_1} \frac{C}{\alpha} \right\}. \tag{82}$$

The conclusion that the composite error vector is uniformly ultimately bounded (UUB) rather than asymptotically convergent to zero is consistent with expectations. In real-world systems, disturbances cannot be estimated and canceled out completely accurately. By controlling the error within a small, acceptable range, the closed-loop system can achieve the desired control objective.

5. Experimental Validation

5.1. Experimental Setup

This paper constructs an experimental platform for a tubular permanent magnet linear synchronous motor, as shown in Figure 3, to physically verify the proposed NNMRAO-MPC control scheme. Mover A is used to verify the position control performance of each control algorithm. Mover B and mover A have identical parameters and are rigidly connected by a mechanical linkage. In the experiment, mover B operates in a closed-loop current mode, outputting a programmable thrust that directly acts on mover A to simulate disturbances, such as sudden load changes and friction fluctuations in real-world operating conditions. The experimental system uses a magnetic grating system for position feedback. The reading head is model MA221030A (Yena Precision Technology Co., Ltd., Shenzhen, China) with a resolution of 1 µm, and the magnetic grating scale is model LM20 (Yena Precision Technology Co., Ltd., Shenzhen, China) with a pitch of 2 mm.

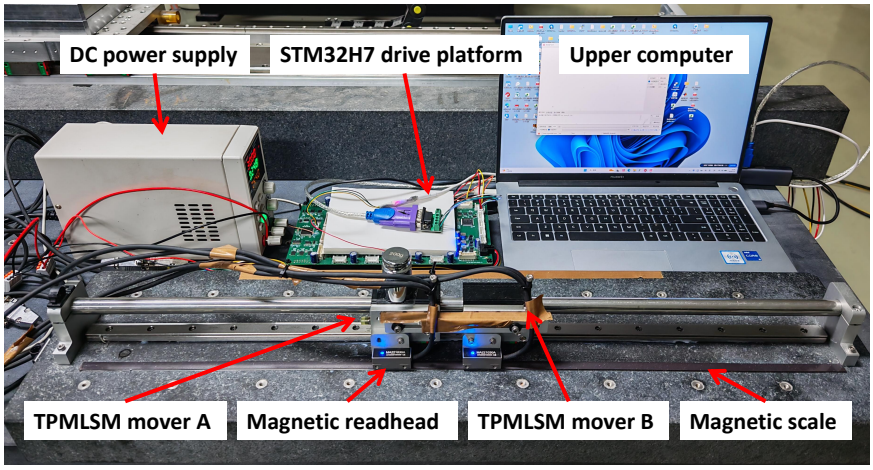


Figure 3. Experimental test platform of TPMLSM.

The actual parameters of the system were obtained through offline identification, and the results are shown in Figure 4. The blue area in the figure represents the identification result after adding 0.2 kg of mass to the existing moving part. It can be seen that the identified mass M also increased by approximately 0.2 kg, so the identification result is reliable. The configuration parameters of the experimental platform are shown in Table 1.

Table 1. Experimental platform parameters.

Parameters	Value	Unit
Effective travel distance	450	mm
Motor pole pitch (N-N)	30	mm
Encoder resolution	1	um
Maximum motor thrust	75	N
Rated current	1.2	Arms
Motor thrust constant	22.0	N/Arms
Mass of moving parts	1.1	kg

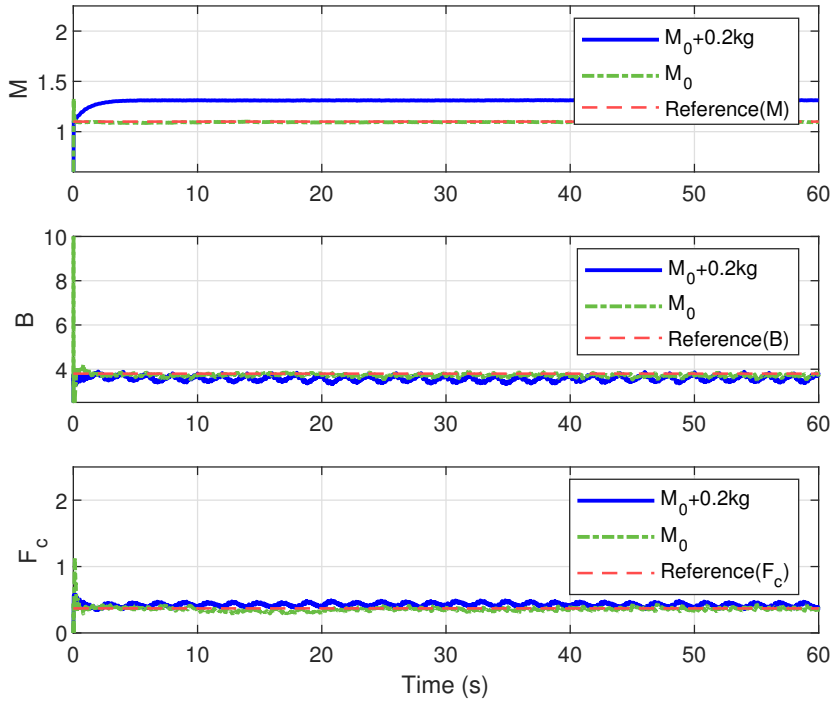


Figure 4. Parameter identification results.

In the experiment, all four controllers were implemented on the same hardware platform. The parameters of each controller underwent extensive experimental testing and iterative adjustments to ensure optimal performance and maintain the fairness of the comparative experiment. The parameters of each control method are as follows:

NNMRAO-MPC: The prediction horizon is set to N_p = 10 and the control horizon to N_c = 5. The state weighting matrix and control weighting matrix are configured as $Q = \text{diag}(500{,}000, 0.01)$ and $R = 0.01$, respectively. Control input upper bound $u_{max} = 60$ N, lower bound $u_{min} = -60$ N, control increment upper bound $\Delta u_{max} = 1$ N, control increment lower bound $\Delta u_{min} = -1$ N. The observer gains are set to $L = \text{diag}(120, 65)$, and the disturbance adaptive update rate is Γ_d = 1,400,000, $\sigma_d = 0.01$. The neural network adopts a three-layer architecture with the number of hidden layer nodes set to $N = 7$, the basis function width set to $\sigma = 1$, and the learning rate set to Γ_W = 1,200,000, $\sigma_W = 0.05$.

MPC: The prediction horizon and weighting matrices are kept identical to those of the NNMRAO-MPC, with the adaptive disturbance observation and compensation module excluded.

SMC: The sliding surface coefficient is set to $c = 600$, the integral coefficient is set to $c_{sum} = 2$, the switching gain coefficients are set to $k_1 = 500$ and $k_2 = 1500$.

PID: The proportional gain of the position loop is set to $K_p = 450$. For the velocity loop, the proportional gain is set to $K_p = 13$, the integral coefficient is set to $K_i = 0.1$, and the feedforward coefficient is set to $K_f = 0.83$.

To fully test and verify the effectiveness of the proposed method, this paper sets up tracking experiments with different trajectories based on actual operating scenarios, and also simulates the disturbance problems encountered in actual operation. External disturbances are realized by mover B in current control mode. A preset step force or sinusoidal force is applied to mover A through mechanical coupling between the two movers, thereby realizing quantitative and repeatable simulation of external load disturbances. During the experiment, a step disturbance i_q^b = 0.05A and a sinusoidal disturbance $i_q^b = 0.05\sin 4\pi t A$ were applied. According to $F = K_f * i_q^b$, the amplitude of the applied disturbance is approximately 1.1N. Without loss of generality, a sinusoidal trajectory $P_{ref} = 0.05\sin \pi t$ (unit: m) and a point-to-point (P2P) trajectory are chosen as the desired trajectory input. The performance of different control strategies is evaluated using the following performance indicators.

RMS (root mean square):

$$L[f]_2 = \sqrt{\frac{1}{N}\sum_{k=1}^{N}(f(k))^2} \tag{83}$$

MAX (maximum value):

$$L[f]_\infty = \max_{k\in[1,N]}(|f(k)|) \tag{84}$$

5.2. Experimental Results Analysis

The verification of all control algorithms in this paper was carried out on a self-developed low-voltage servo driver. The main control chip was an STM32H723 (STMicroelectronics, Geneva, Switzerland) with a main frequency of 550 MHz, equipped with a double-precision FPU and supporting a matrix library. The three-phase full-bridge inverter used an N-channel MOSFET IPG20N06S4L-26 (Infineon Technologies, Neubiberg, Germany). The current was sampled through the lower bridge sampling resistor, amplified by the operational amplifier TL072, and then sampled by the MCU's built-in high-speed ADC. The MPC optimization problem solved using qpOASES [43]. The execution time of each module is summarized in Table 2. The current loop runs at 10 kHz within a hardware timer interrupt, with a single execution time of approximately 5 μs. The outer position/velocity control loop operates at 1 kHz, and within each 1 ms control cycle, the NNMRAO update takes approximately 42 μs, the MPC optimization problem solution takes approximately 100 μs, and other tasks including velocity/position computation and trajectory planning are also completed sequentially, with a combined execution time of approximately 171 μs, thereby satisfying the real-time control requirements. Experimental results demonstrate that the proposed algorithm is fully real-time implementable on the existing embedded hardware platform.

Table 2. Computational real-time performance parameters of each control modules.

Module	Execution Period	Execution Time	Time Ratio (%)
Current Loop	100 μs	5.1 μs	5.1%
NNMRAO Observer Update	1000 μs	42.4 μs	4.24%
MPC Online Solver	1000 μs	100.2 μs	10.02%
Position Loop (Total)	1000 μs	171.2 μs	17.12%

First, a static disturbance experiment was conducted, with the target position set to 0 m. After the system stabilizes, a step disturbance of 0.05 A and a sinusoidal disturbance of 0.05 A with a frequency of 4 Hz are applied at t = 10 s, respectively, and the disturbance lasts for 10 s. The introduction of sinusoidal disturbances does not conflict with the assumption of slow change of d_0 in the previous derivation of the disturbance observer. According to the time separation principle [44], the frequency of position control is much greater than the frequency of sinusoidal disturbances, so the amplitude of disturbance change is small within adjacent discrete control cycles. Furthermore, according to Equation (40), the time-varying nonlinear part of the lumped disturbance will be incorporated into d_n and estimated online by RBF. Figures 5–10 show the position response, control output, and NNMRAO disturbance estimation curves of the four control methods under different disturbances.

The experimental results for step disturbances are shown in Figures 5–7. At the moment the disturbance is applied, both the PID and SMC generate large transient peak deviations. Subsequently, they gradually converge to the target value by relying on feedback adjustment. The convergence speed is slow and accompanied by obvious damped oscillations. The standard MPC has a small transient peak deviation, but there will be a persistent steady-state error during the application of disturbances. NNMRAO-MPC exhibits the smallest transient deviation and converges rapidly to the reference position in a very short time, with steady-state error approaching zero, demonstrating the best step disturbance rejection performance. Figure 7 shows the disturbance estimate from NNMRAO, showing that the observer can closely estimate the amplitude and variation of the disturbance. Due to the presence of unmodeled disturbances, the observed disturbance cannot perfectly coincide with the applied ideal disturbance. The above results show that NNMRAO can achieve rapid identification of step disturbances. Substituting the disturbance into MPC effectively suppresses transient biases and eliminates steady-state errors caused by model mismatch in standard MPC.

The experimental results for sinusoidal disturbances are shown in Figures 8–10. It can be seen that the oscillation amplitude of the PID is the largest during the disturbance application phase, and it is consistent with the frequency of the external sinusoidal disturbance. It relies entirely on feedback correction and has weak suppression capability for unknown disturbances. The SMC controller shows a slight improvement in oscillation amplitude compared to the PID controller. The oscillation amplitude of standard MPC is similar to that of SMC, but since the prediction model does not contain disturbances, the residual error persists with the disturbances. The position curve of NNMRAO-MPC always closely follows the reference value, and the steady-state oscillation amplitude is minimal. After the disturbance is removed, both the PID controller and the SMC controller can quickly return to the reference value. The standard MPC controller exhibits significant noise and steady-state errors, while the NNMRAO-MPC controller's observer output rapidly converges to a smaller value after the disturbance is removed, and its position smoothly returns to the reference value. These experimental results demonstrate the fast tracking and stable characteristics of the proposed control method under disturbance changing scenarios.

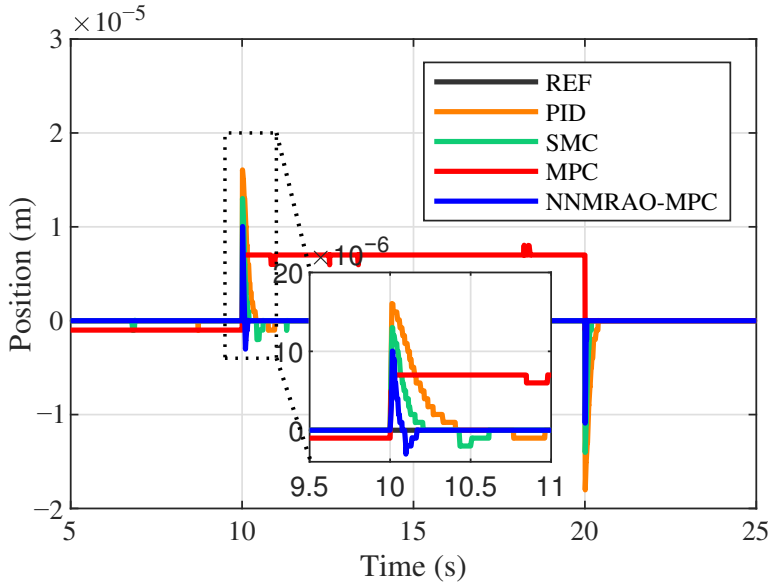


Figure 5. Steady-state step disturbance position.

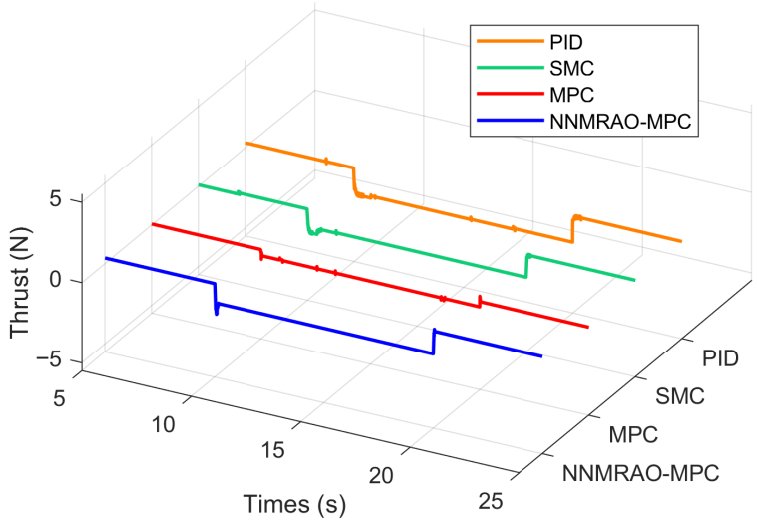


Figure 6. Steady-state step disturbance control input.

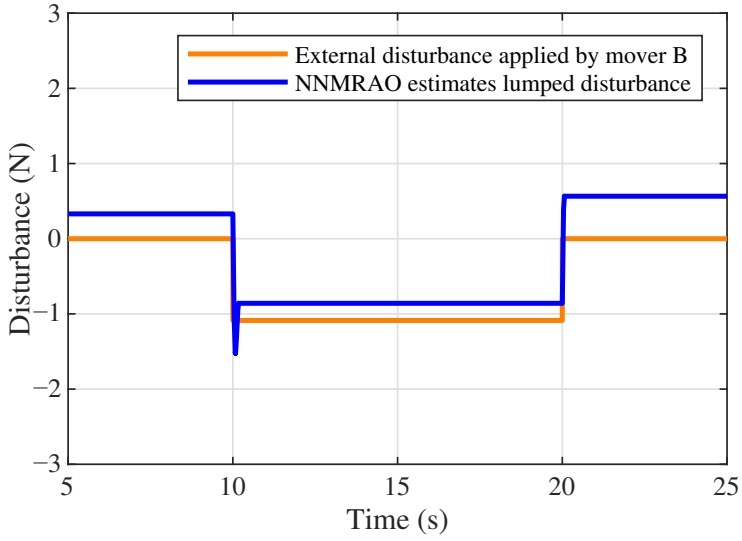


Figure 7. Estimated value of steady-state step disturbance.

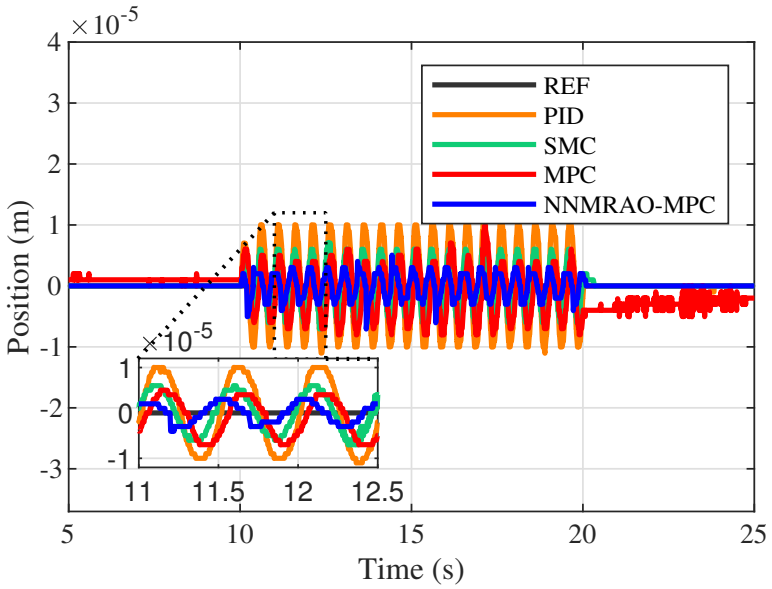


Figure 8. Steady-state sinusoidal disturbance position.

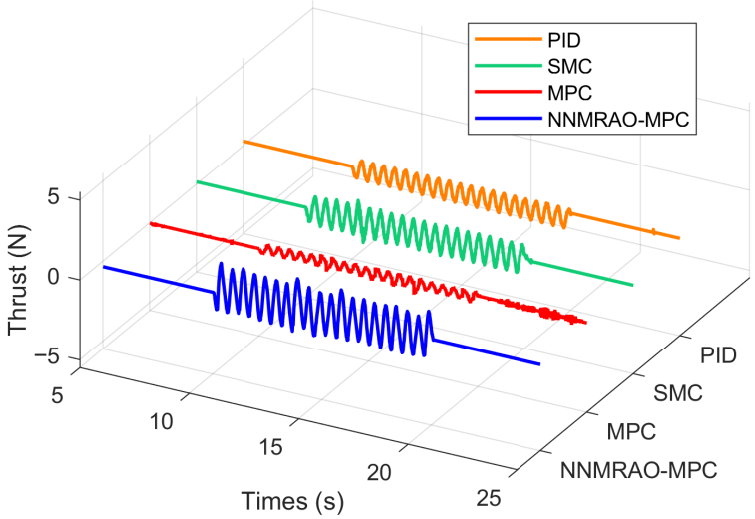


Figure 9. Steady-state sinusoidal disturbance control input.

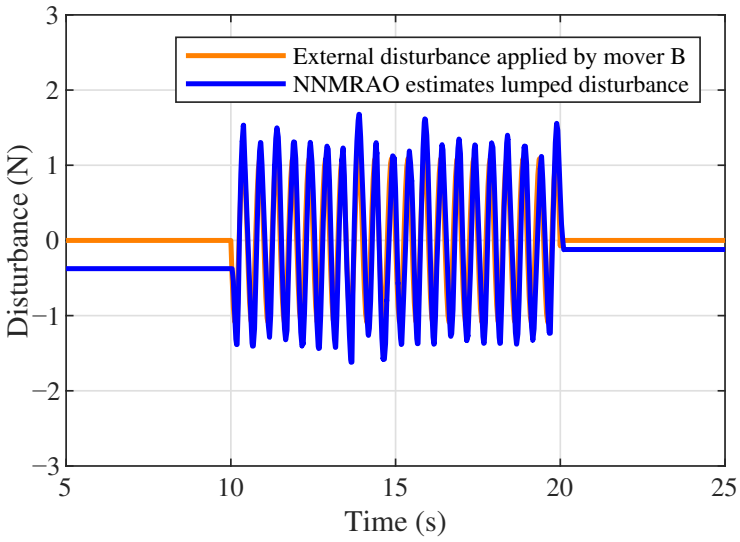


Figure 10. Disturbance estimate of steady-state sinusoidal disturbance.

Figures 11–18 show the position tracking experimental results of different control methods under two kinds of reference trajectories. In the trajectory tracking experiment, the data acquisition range was 0–60 s. To better display the details, the plotting range for position tracking and disturbance estimation was 0–12 s, while the plotting range for the other states was 0–60 s. The details of test track tracking of different control methods are shown in Figures 11 and 15. Compared with the traditional PID control method, SMC, MPC and NNMRAO-MPC show better tracking performance. Figures 12 and 16 show the waveforms of the tracking error. The PID error has the largest amplitude and exhibits obvious periodic fluctuations, while the SMC and MPC errors are lower in amplitude compared to the PID. The proposed NNMRAO-MPC error peak is significantly reduced and remains within a small range. The control output is shown in Figures 13 and 17. It can be seen that the amplitude and fluctuation of PID control input signal are large, and the control input using IMPC is relatively smooth. The disturbance estimation results of MRAO are shown in Figures 14 and 18. It can be seen that the the disturbance obtained by the observer is approximately consistent with the amplitude and period of the applied disturbance, with minor discrepancies due to unmodeled dynamics. The results demonstrate that the proposed method successfully estimates and compensates for unknown disturbances, achieving enhanced precision in trajectory tracking.

Based on the calculation results within the steady-state range of 10 s $\leq t \leq$ 50 s, Table 3 presents the quantitative performance indicators of the four control methods under two types of reference trajectories. It can be seen that the NNMRAO-MPC method achieves smaller overall tracking error and peak error under both Sine and P2P trajectories. Compared with the conventional MPC, the proposed NNMRAO-MPC achieves reductions in RMS of 76.09% and 78.85% under the two evaluated trajectories in the presence of unknown disturbances, with corresponding maximum tracking errors reduced by 56.38% and 64.11%, respectively. Compared to traditional MPC, the online disturbance compensation method proposed in this article does not introduce additional control peaks, indicating that the improved position tracking performance does not come at the cost of amplified control input. In summary, the NNMRAO proposed in this article achieves approximate compensation for parameter uncertainties and unknown disturbances, thereby improving the control accuracy of MPC. IMPC makes the control input smooth, without significant control signal amplification or high-frequency oscillation problems. Experimental results show that, compared with the baseline controller without explicit disturbance estimation, the proposed method significantly reduces the tracking error caused by disturbances and achieves high-precision trajectory tracking.

Table 3. Performance Indicators in Experiment.

Traj	Index Units	$L[e]_2$ μm	$L[e]_\infty$ μm	$L[u]_2$ N	$L[u]_\infty$ N
Sine	NNMRAO-MPC	5.457	25.52	1.368	4.064
	MPC	22.82	58.51	1.377	3.992
	SMC	13.48	40.42	1.396	4.728
	PID	37.46	76.17	1.612	4.358
P2P	NNMRAO-MPC	4.565	22.68	1.247	4.198
	MPC	21.58	63.20	1.862	3.513
	SMC	11.51	35.15	1.190	3.966
	PID	24.09	60.48	1.403	4.175

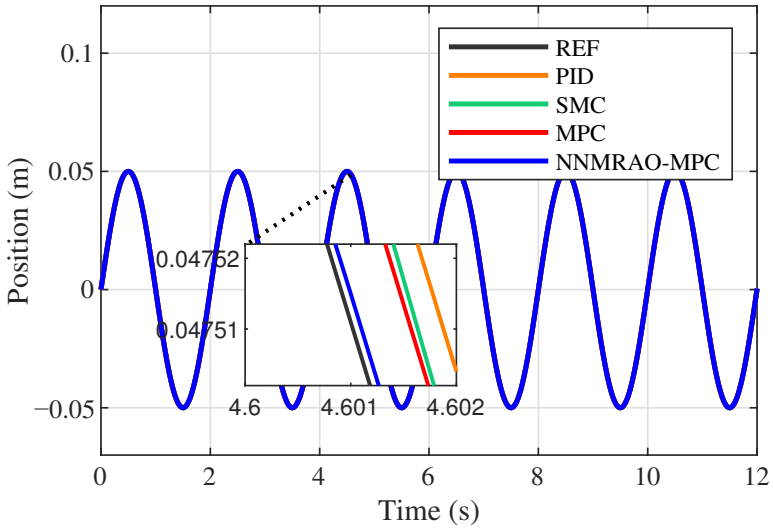


Figure 11. Sinusoidal trajectory tracking position.

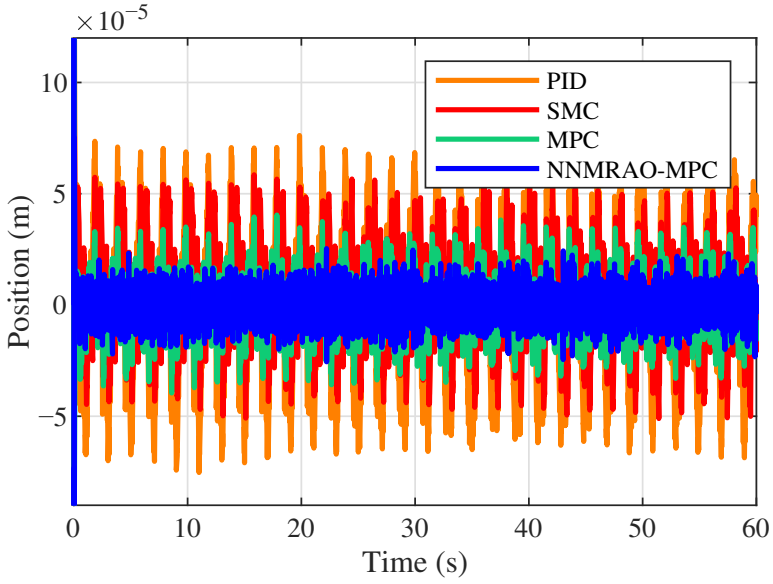


Figure 12. Sinusoidal trajectory tracking error.

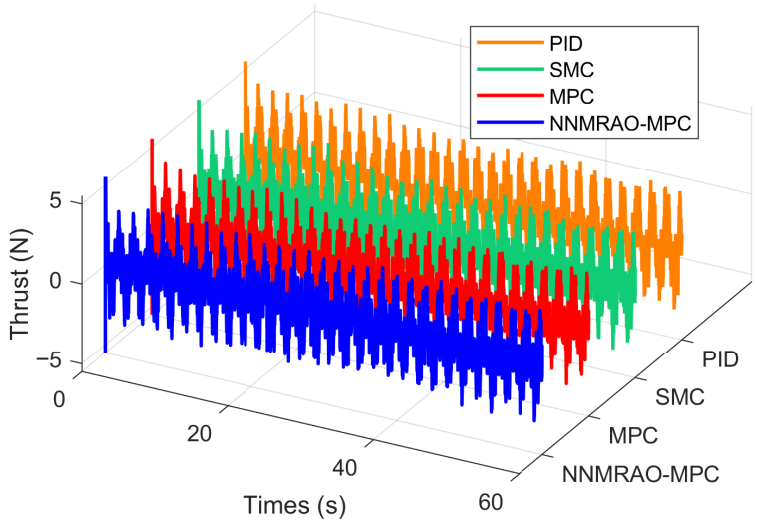


Figure 13. Sinusoidal trajectory control input.

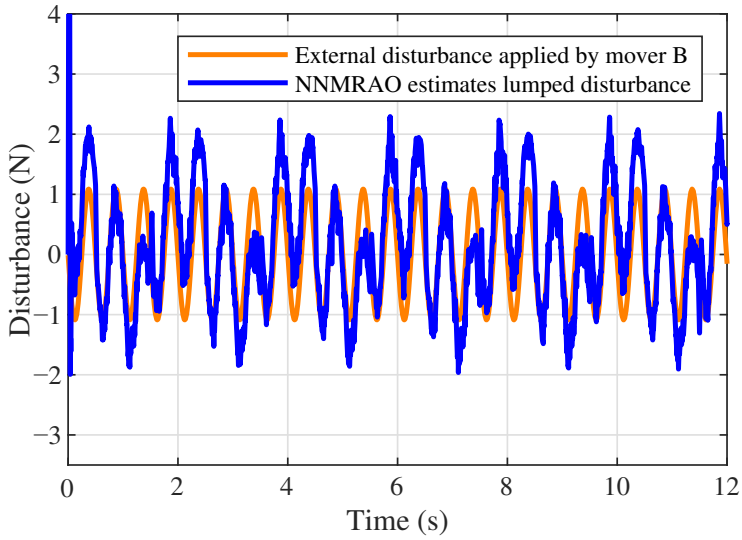


Figure 14. Estimated disturbance of sinusoidal trajectory.

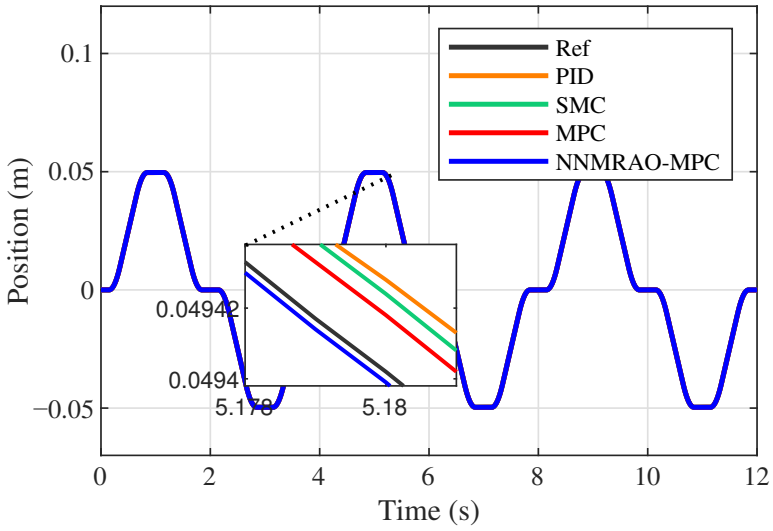


Figure 15. Point to point trajectory tracking position.

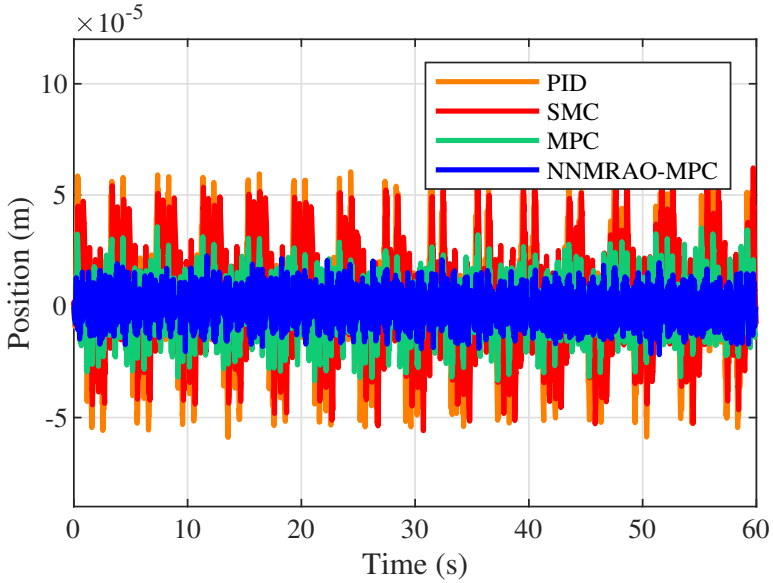


Figure 16. Point to point trajectory tracking error.

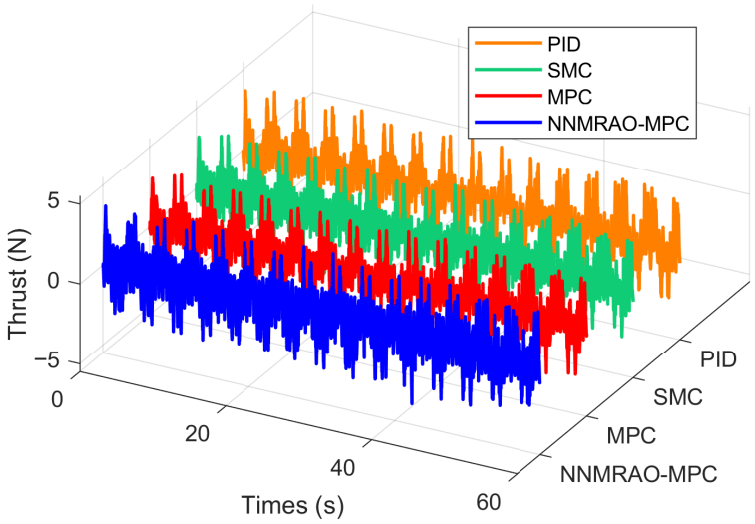


Figure 17. Point to point trajectory control input.

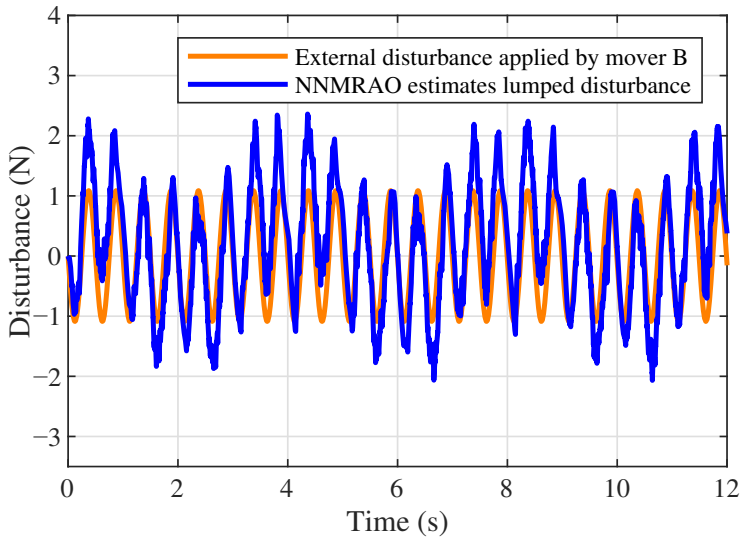


Figure 18. Estimated disturbance of point-to-point trajectory.

6. Conclusions

In this article, a new disturbance extended model predictive position control method based on NNMRAO is proposed for the position tracking control of TPMLSM. The neural network is embedded in MRAO to enhance the estimation ability of the observer for nonlinear high-frequency disturbances. The estimated disturbance is explicitly introduced into MPC as an extended state to realize the online estimation and compensation of disturbance. Compared with conventional MPC, the proposed method effectively suppresses unknown disturbances and improves trajectory tracking accuracy on the TPMLSM experimental platform used in this study. Extensive comparative experiments under different reference trajectories and disturbance scenarios confirm the effectiveness of the proposed method for this class of motor. However, the calculation of neural network and model prediction is time-consuming. How to improve the computational efficiency and make it suitable for more embedded scenarios is one of the main directions of future research.

Author Contributions: Methodology, Y.Z. and Z.L.; Software, R.Q.; Validation, Y.Z.; Data curation, R.Q.; Writing—original draft, Y.Z.; Writing—review and editing, Z.L.; Funding acquisition, Z.L. All authors have read and agreed to the published version of the manuscript.

Funding: This work was supported in part by the National Natural Science Foundation of China, grant numbers 62533017 and 62403172, and in part by the Natural Science Foundation of Heilongjiang Province of China, grant number YQ2025F006.

Institutional Review Board Statement: Not applicable.

Informed Consent Statement: Not applicable.

Data Availability Statement: The data that support the findings of this study are available from the corresponding author upon reasonable request.

Conflicts of Interest: The authors declare no conflicts of interest.

References

1. Khosravi, M.; König, C.; Maier, M.; Smith, R.S.; Lygeros, J.; Rupenyan, A. Safety-aware cascade controller tuning using constrained Bayesian optimization. *IEEE Trans. Ind. Electron.* **2022**, *70*, 2128–2138. [CrossRef]
2. Balula, S.; Liao-McPherson, D.; Rupenyan, A.; Lygeros, J. Data-driven reference trajectory optimization for precision motion systems. *Control Eng. Pract.* **2024**, *144*, 105834. [CrossRef]
3. Zhang, T.; Li, X.; Gai, H.; Zhu, Y.; Cheng, X. Integrated controller design and application for CNC machine tool servo systems based on model reference adaptive control and adaptive sliding mode control. *Sensors* **2023**, *23*, 9755. [CrossRef]
4. Yuan, M.; Chen, Z.; Yao, B.; Liu, X. Fast and accurate motion tracking of a linear motor system under kinematic and dynamic constraints: An integrated planning and control approach. *IEEE Trans. Control Syst. Technol.* **2019**, *29*, 804–811. [CrossRef]
5. Zhao, Y.; Liu, Z.; Yu, X.; Qiu, J.; Rodríguez-Andina, J.J. Surrogate Model-Assisted Robust Multiobjective Optimization of Equivalent Halbach Array Tubular Permanent Magnet Linear Synchronous Motors. *IEEE Trans. Ind. Electron.* **2026**, 1–10. [CrossRef]
6. Tornai, T.; Simon, J.; Gogolák, L.; Fürstner, I. Accuracy Evaluation of a Linear Servo Positioning System. *Actuators* **2025**, *14*, 613. [CrossRef]
7. Wang, X.; Chen, F.; Zhu, R.; Huang, X.; Sang, N.; Yang, G.; Zhang, C. A Review on Disturbance Analysis and Suppression for Permanent Magnet Linear Synchronous Motor. *Actuators* **2021**, *10*, 77. [CrossRef]
8. Yuan, S.; Yi, W.; Yang, G. Adaptive robust control of electromagnetic actuators with friction nonlinearity and uncertainty compensation. *Math. Model. Eng.* **2024**, *10*, 75–86. [CrossRef]
9. Bascetta, L.; Rocco, P.; Magnani, G. Force ripple compensation in linear motors based on closed-loop position-dependent identification. *IEEE/ASME Trans. Mechatron.* **2009**, *15*, 349–359. [CrossRef]
10. Liu, Y.; Zhang, L.; Li, P.; Xu, Y. Active Disturbance Rejection for Linear Induction Motors: A High-Order Sliding-Mode-Observer-Based Twisting Controller. *Actuators* **2025**, *14*, 200. [CrossRef]
11. Kang, K.; Wang, M.; Sun, J.; Zhang, C.; Li, L. Nonlinear friction compensation for PMLSM using an enhanced adaptive friction observer. *IEEE Trans. Ind. Electron.* **2024**, *71*, 16234–16244. [CrossRef]
12. Hernandez-Guzman, V.; Carrillo-Serrano, R.V. Global PID position control of PM stepper motors and PM synchronous motors. *Int. J. Control* **2011**, *84*, 1807–1816. [CrossRef]
13. Liu, Y.C. Disturbance-observer-based second-order sliding-mode position control for permanent-magnet synchronous motors: A continuous twisting algorithm-based approach. *Energies* **2024**, *17*, 2974. [CrossRef]
14. Xu, Y.; Huang, Z.; Liu, D. Research on Position Tracking Performance Optimization of Permanent Magnet Synchronous Motors Based on Improved Active Disturbance Rejection Control. *Appl. Sci.* **2025**, *15*, 10467. [CrossRef]
15. Liu, Z.; Gao, H.; Yu, X.; Lin, W.; Qiu, J.; Rodriguez-Andina, J.J.; Qu, D. B-spline wavelet neural-network-based adaptive control for linear-motor-driven systems via a novel gradient descent algorithm. *IEEE Trans. Ind. Electron.* **2023**, *71*, 1896–1905. [CrossRef]
16. Dong, H.; Yang, X.; Basin, M.V. Practical tracking of permanent magnet linear motor via logarithmic sliding mode control. *IEEE/ASME Trans. Mechatron.* **2022**, *27*, 4112–4121. [CrossRef]
17. Liu, Z.; Zhang, Z.; Lin, W.; Yu, X.; Buccella, C.; Cecati, C. Disturbance rejection-based motion control of linear motors via integral sliding mode observer. *IEEE Trans. Ind. Electron.* **2024**, *72*, 3061–3071. [CrossRef]
18. Li, Z.; Wang, K.; Wang, J.; Zhang, L.; Sun, H. Full-coefficient intelligent adaptive position control of permanent magnet synchronous linear motor. *J. Electr. Eng. Technol.* **2023**, *18*, 1975–1984. [CrossRef]
19. Liu, X.; Zhen, S.; Sun, H.; Zhao, H. A novel model-based robust control for position tracking of permanent magnet linear motor. *IEEE Trans. Ind. Electron.* **2019**, *67*, 7767–7777. [CrossRef]
20. Ling, J.; Feng, Z.; Chen, L.; Zhu, Y.; Pan, Y. Neural network-based iterative learning control of a piezo-driven nanopositioning stage. *Precis. Eng.* **2023**, *81*, 112–123. [CrossRef]
21. Liu, Z.; Zhong, H.; Lin, X.; Yu, X.; Rodríguez-Andina, J. Integrated Motion Control Framework of Wheel-Legged Biped Robot on Rugged Terrain. *IEEE/ASME Trans. Mechatron.* **2025**, *30*, 7383–7394. [CrossRef]

22. Cao, W.; Qiao, J. Piecewise Iterative learning control for linear motors under random initial position. *J. Frankl. Inst.* **2025**, *362*, 107578. [CrossRef]
23. Chai, S.; Wang, L.; Rogers, E. Model predictive control of a permanent magnet synchronous motor with experimental validation. *Control. Eng. Pract.* **2013**, *21*, 1584–1593. [CrossRef]
24. Guo, Q.; Pan, T.; Liu, J.; Chen, S. Explicit model predictive control of permanent magnet synchronous motors based on multi-point linearization. *Trans. Inst. Meas. Control* **2021**, *43*, 2872–2881. [CrossRef]
25. Karimi, M.; Rostami, M.A.; Zamani, H. Continuous control set model predictive control for the optimal current control of permanent magnet synchronous motors. *Control Eng. Pract.* **2023**, *138*, 105590. [CrossRef]
26. Cui, S.; Wu, J.; Cai, S.; Wei, Y.; Wang, Z.; Wang, X. Current prediction control methods for permanent magnet synchronous motor models: A review. *Int. J. Dyn. Control* **2026**, *14*, 77. [CrossRef]
27. Liu, K.; Zhang, Q.; Zhu, Z.Q.; Zhang, J.; Shen, A.W.; Stewart, P. Comparison of two novel MRAS based strategies for identifying parameters in permanent magnet synchronous motors. *Int. J. Autom. Comput.* **2010**, *7*, 516–524. [CrossRef]
28. Liu, X.; Pan, Y.; Wang, L.; Xu, J.; Zhu, Y.; Li, Z. Model predictive control of permanent magnet synchronous motor based on parameter identification and dead time compensation. *Prog. Electromagn. Res. C* **2022**, *120*, 253–263. [CrossRef]
29. Bai, C.; Yin, Z.; Zhang, Y.; Liu, J. Robust predictive control for linear permanent magnet synchronous motor drives based on an augmented internal model disturbance observer. *IEEE Trans. Ind. Electron.* **2022**, *69*, 9771–9782. [CrossRef]
30. Wang, Y.; Liu, X. Model predictive position control of permanent magnet synchronous motor servo system with sliding mode observer. *Asian J. Control* **2023**, *25*, 443–461. [CrossRef]
31. Brosch, A.; Wallscheid, O.; Böcker, J. Long-term memory recursive least squares online identification of highly utilized permanent magnet synchronous motors for finite-control-set model predictive control. *IEEE Trans. Power Electron.* **2022**, *38*, 1451–1467. [CrossRef]
32. Brosch, A.; Hanke, S.; Wallscheid, O.; Böcker, J. Data-driven recursive least squares estimation for model predictive current control of permanent magnet synchronous motors. *IEEE Trans. Power Electron.* **2020**, *36*, 2179–2190. [CrossRef]
33. Jiang, C.; Yang, J.; Li, S.; Zhou, M.; Yang, K. Friction-compensation and extended state observer based model predictive control for PMSM servo systems. *IEEE J. Ind. Appl.* **2020**, *9*, 351–357. [CrossRef]
34. Mayne, D.Q.; Rawlings, J.B.; Diehl, M.M. *Model Predictive Control: Theory, Computation, and Design*, 2nd ed.; Nob Hill Pub: San Francisco, CA, USA, 2024.
35. Powell, J.D.; Workman, M.L. *Digital Control of Dynamic Systems*; Addison-Wesley: Reading, MA, USA, 2002.
36. Zhao, F.; Gupta, Y.P. A simplified predictive control algorithm for disturbance rejection. *ISA Trans.* **2005**, *44*, 187–198. [CrossRef] [PubMed]
37. Kim, Y.H.; Lewis, F.L.; Abdallah, C.T. A dynamic recurrent neural-network-based adaptive observer for a class of nonlinear systems. *Automatica* **1997**, *33*, 1539–1543. [CrossRef]
38. Lewis, F.; Jagannathan, S.; Yesildirak, A. *Neural Network Control of Robot Manipulators and Non-Linear Systems*; CRC Press: Boca Raton, FL, USA, 2020.
39. Ogata, K. *Modern Control Engineering*; Prentice Hall: Upper Saddle River, NJ, USA, 2010.
40. Horn, R.A.; Johnson, C.R. *Matrix Analysis*; Cambridge University Press: Cambridge, UK, 2012.
41. Steele, J.M. *The Cauchy-Schwarz Master Class: An Introduction to the Art of Mathematical Inequalities*; Cambridge University Press: Cambridge, UK, 2004.
42. Khalil, H.K. *Nonlinear Systems*, 3rd ed.; Prentice Hall: Upper Saddle River, NJ, USA, 2002.
43. Ferreau, H.J.; Kirches, C.; Potschka, A.; Bock, H.G.; Diehl, M. qpOASES: A parametric active-set algorithm for quadratic programming. *Math. Program. Comput.* **2014**, *6*, 327–363. [CrossRef]
44. Chen, W.H.; Yang, J.; Guo, L.; Li, S. Disturbance-observer-based control and related methods—An overview. *IEEE Trans. Ind. Electron.* **2015**, *63*, 1083–1095. [CrossRef]

Disclaimer/Publisher's Note: The statements, opinions and data contained in all publications are solely those of the individual author(s) and contributor(s) and not of MDPI and/or the editor(s). MDPI and/or the editor(s) disclaim responsibility for any injury to people or property resulting from any ideas, methods, instructions or products referred to in the content.